Gjengedal et al. International Journal of Mechanical and Materials Engineering (2021) 16:10
https://doi.org/10.1186/s40712-021-00132-8

International Journal of Mechanical and Materials Engineering

ORIGINAL PAPER Open Access

Prediction of buckling force in hourglass-shaped specimens

Ragnar Gjengedal[1*], Ørjan Fyllingen[2] and Vojtech Heinik[3]

Abstract

It is important to avoid buckling during low-cycle fatigue testing. The buckling load is dependent on the specimen shape, material properties, and the testing machine. In the present investigation of hourglass-shaped specimens the importance of the diameter to radius of curvature is examined. Diameters of 5 and 7 mm are examined with a ratio of radius of curvature to diameter of 4, 6, and 8. The machine used is an Instron 8800 with elongated rods for a climate chamber. This leads to a reduced stiffness of the machine during compression testing. A finite element model (in Abaqus) is developed to identify the critical buckling force. For hourglass-shaped specimens, buckling means onset of sideways movement, without a drop in the applied load which is typical for conventional Euler buckling. The onset of sideways movement is identified experimentally by analysis of the data from extensometer and the load cell. This model is verified by experiments and fits within 0.6 to − 11% depending on the specimen diameter and diameter to radius of curvature ratio. The smallest deviations are obtained for the 7-mm-diameter specimen with deviation varying from 0.6 to − 3.3% between the model and the experiments. The current investigation is done with a commercially available hot rolled structural steel bar of Ø16 mm.

Keywords: Compression testing, Hourglass specimen design, Finite element modeling, Critical buckling force, Hot rolled steel, Low-cycle fatigue

Introduction

Specimen design due to fatigue testing machine construction limits are not well described in the literature. Therefore, a method to identify the limits for an actual machine is needed. During axial low-cycle fatigue testing, one has to make sure that this buckling is avoided in the compression cycle. Hourglass-shaped specimens are suited to investigate low-cycle fatigue. The hourglass shape is suitable to resist buckling during the compression phase compared to a uniform section specimen. It is time-consuming to determine the onset of buckling by experiments alone and buckling might damage the laboratory equipment. Therefore, one needs to find a method to calculate the critical buckling force, i.e., the onset of sideways movement during the compression cycle. This is different from Euler buckling as this kind of buckling occurs at a force lower than maximum force. During Euler buckling, a sudden drop in force is observed. For an hourglass-shaped specimen, buckling (the onset of sideways movement) is observed without a sudden drop in force. This paper shows a method developed to calculate this critical buckling force and experiments to verify the model.

In the literature, there are limited descriptions of specimen design for low-cycle fatigue specimens by a finite element model and corresponding verification by experiments. The paper of Sandhya et al. (1994) gives a valuable description of experiments with different specimen geometries. Narendra et al. (2019) investigated low-cycle fatigue behaviour and cyclic placiticty of mild steel. Hales et al. (2014) presented a code of practice for the determination of cyclic stress-strain data. Nogami et al. (2010) studied the effect of specimen shape on the low-cycle fatigue life of small specimens. The investigation includes the results of finite element model. Skelton

* Correspondence: rgje@hvl.no
[1]Mechanical Engineering, Western Norway University of Applied Sciences, 5063 Bergen, Norway
Full list of author information is available at the end of the article

(2013) describes tests with different R/d ratios and a parallel section of the specimen.

The design of low-cycle fatigue specimen is of great importance when it comes to setting up reproducible tests. Therefore, the standard from the American Society of Testing and Materials, ASTM E606/606M (2012), has been used as a guideline for the specimen geometry. In the current investigation, specimens were designed with a R/d ratio from 4 to 8, which is well defined by ASTM E606/606M (2012). A conventional mild low-carbon steel was used. In order to identify the onset of buckling, an examination of the flexibility (the derivative of elongation to force) was analyzed from experimental data, as conventional buckling is associated with a rapid change in strain and/or force. To predict the critical buckling force, finite element models were made using the finite element code (Abaqus Dassault Systèmes®). The material model in the commercially available code (Abaqus) was calibrated based on tensile tests of the material. The model was validated by experimental tests in order to verify the critical buckling force for the actual material.

In this work, the specimens were tested in an Instron servo-hydraulic testing machine (Instron 8800). The specific machine is equipped with a climate chamber for testing temperatures ranging from − 70 to 350 °C and therefore has elongated rods for the allowance of the specimen mounting heads inside the chamber. This gives a wide experimental range. The elongation rods are treaded onto the piston rod of the machine. Thereby, some mechanical flexibility is introduced. However, the experiments must be designed so that buckling is avoided during the compression phase of the cycle.

Methods and experimental design

Material, constitutive model, and parameter identification

The material used for these tests is a commercial quality hot rolled structural steel S355J2-1.0577. The specimens were machined from a Ø = 16-mm bar which were approved according to EN10025-1 (2004). The minimum required yield strength is 355 MPa and the ultimate tensile strength is within 510-680 MPa according to EN10025-1 (2004). A computer numerical controlled (CNC) lathe was used to machine the specimens. A high-quality surface finish is not considered to be critical for the onset of buckling in a one-cycle compression test.

The material model is based on von Mises yield criterion, the associated flow rule, and a modified Voce law. Calibration was based on tensile tests. Design of the tensile specimens was done according to Fig. 1. Diameters were measured on the individual specimens tested. Three specimens in parallel were tested. The deformation of the specimens was measured by a longitudinal extensometer with a gage length of 12.5 mm. The tensile experiments were displacement controlled. A rate of 1.56 mm/min were used and a sampling frequency of 20 Hz. The strain was logged from machine displacement in addition to the longitudinal extensometer.

The variation between the stress-strain curves of the specimens tested was minimal. Results from one of the tensile tests are described in Fig. 2. The true stress-true strain and engineering stress -engineering strain curves are shown.

In order to include the yielding plateau, Voce law had to be modified by a constant to include the strain at the end of the yield plateau ε_0.

$$\sigma_{(\varepsilon p)} = \sigma_{ys}, \varepsilon_p \leq \varepsilon_0$$

$$\sigma_{(\varepsilon p)} = \sigma_{ys} + \sum_{i=1}^{n} Q_i \cdot \left(1 - e^{\left(-C_i \cdot \left(\varepsilon_p - \varepsilon_0\right)\right)}\right), \varepsilon_p > \varepsilon_0$$

where the parameters:

σ_{ys} is yield stress measured from the test.

ε_0 is plastic strain at the end of the yielding plateau.

Q_i and C_i are constants calculated from experimental data by applying least square method.

By applying n = 2, the Voce law fitted the experimental data well. This can be seen in Fig. 3. The parameters of the Voce rule were calibrated by minimizing the following error (least square fit) by using the problem solver in spreadsheet (Excel):

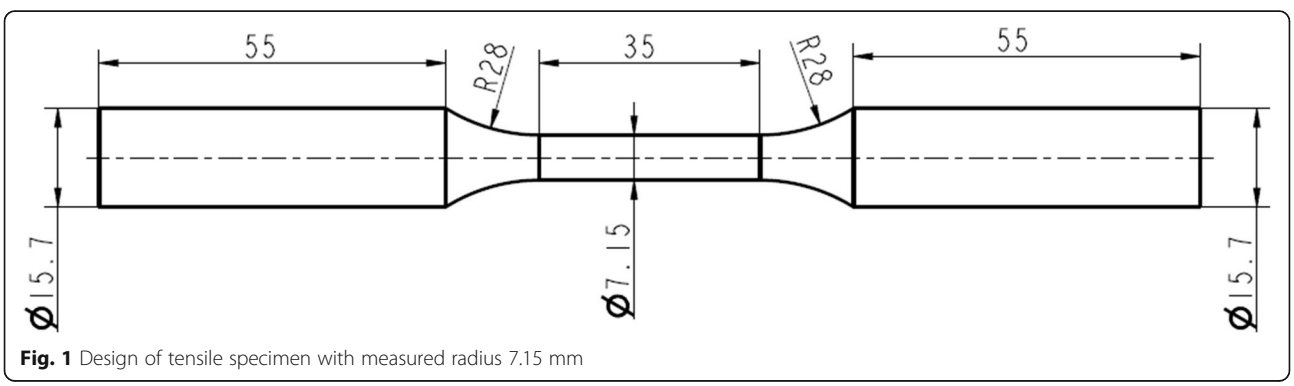

Fig. 1 Design of tensile specimen with measured radius 7.15 mm

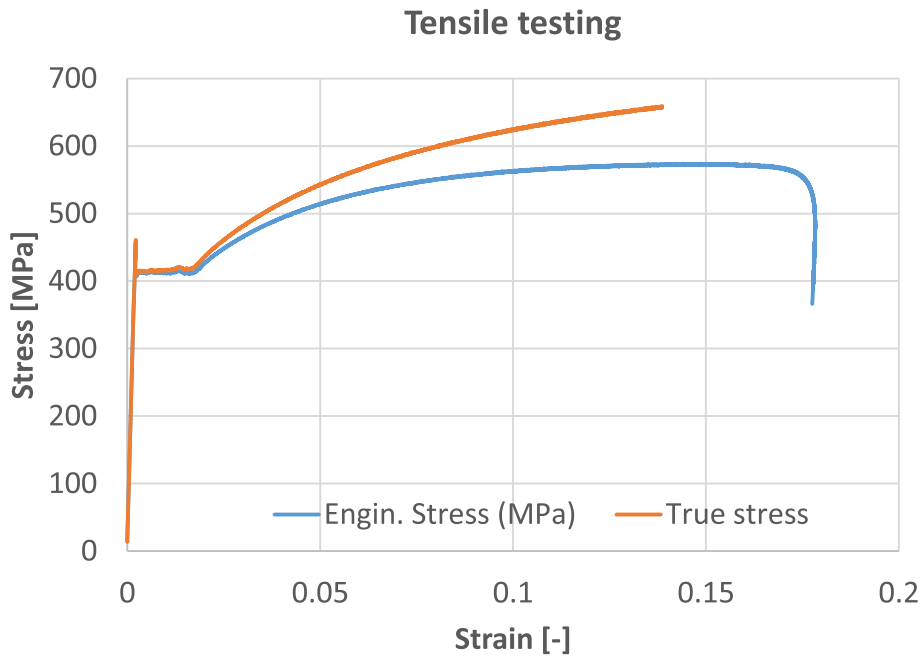

Fig. 2 Engineering stress and true stress from tensile testing

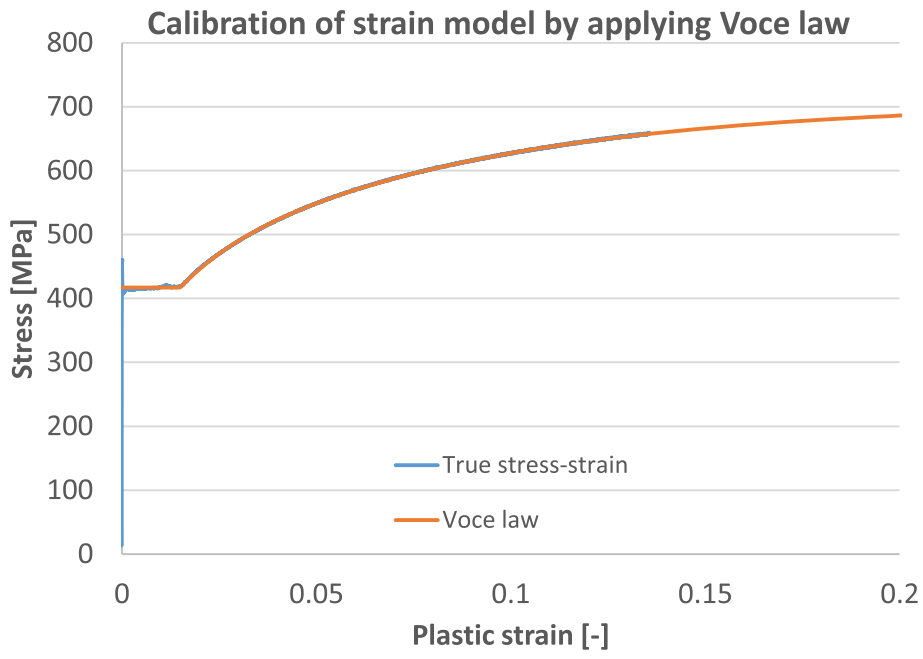

Fig. 3 Calibration of material model by applying Voce law

$$Error = \sum_{i=1}^{k} \left(\sigma_i - \sigma^*\left(\varepsilon_{pi}\right)\right)^2$$

where σ_i is the measured true stress at data point i.

σ^* (ε_{pi}) is the calculated stress at the plastic strain at data point i.

k is the total number of data points used for the calibration.

The values obtained from the calibration are described in Table 1.

One can see from Fig. 3 that the Voce law model extrapolated further than the true stress-strain curve. This is because the true stress-true strain curve is only valid onto the onset of diffuse necking in elongation.

Experimental design

The tests were designed according to ASTM E606/606M (2012). This standard describes various geometries allowed for strain-controlled fatigue testing. This is used also for low-cycle fatigue testing. Servo-hydraulic machines are widely used for fatigue testing of steel and other high strength materials. The machine with a specimen mounted is shown in Fig. 4. For low-cycle fatigue testing the uniform specimen is not suited due to a substantial lower buckling force. Hourglass-shaped specimens are therefore better suited for low-cycle fatigue testing. The geometries tested varied with R/d ratio between the diameter and the radius of curvature as described in Fig. 5 for a general setup. The grips were circular without treads. Compression was done with specimens according to Figs. 5 and 6. Table 2 describes the different diameters and ratios used in the tests. The overall length of the specimens was larger than the prescribed values of 20 days + 4 days. This extra length was confined within the grips, so that we also could fit the longitudinal extensometer onto the specimen during testing.

Finite element model

The design of a finite element model is essential in order to predict the experimental behavior. Initially, a model for the whole machine and the specimen was made using a finite element code (Abaqus). This introduced several factors to the model that lead to assumptions and uncertainties. Such a model requires also a substantial amount of run-time of a strong computer. Therefore, a simplified model was developed, which is described in Fig. 7 (part a). It was chosen to use the explicit solver, which is commonly used to solve dynamic problems. However, the explicit method is also used in the literature to solve quasistatic problems similar to the one in this investigation shown by Romanova et al. (2019) and Hu et al. (1994). Full three-dimensional models must be made in order to capture the buckling behavior. Convergence tests of the 3D model were done by refining the element mesh until insignificant difference from the previous mesh size. In addition, an axisymmetric model in tension was modeled with a fine mesh and compared to the 3D model with the mesh used in the modeling of the compression tests. The time of the simulation was set to 1 s. This gave a sufficiently low speed of the deformation to ensure that the kinetic energy was insignificant compared to the total energy. The element chosen was the C3D8R element (8-node linear brick, reduced

Table 1 Calibration values from the tests

$\sigma_o = R_e$ [MPa]	417
ε_0	0.015
n	2
Q1 [MPa]	44.51
Q2 [MPa]	246.17
C1	70.59
C2	13.18

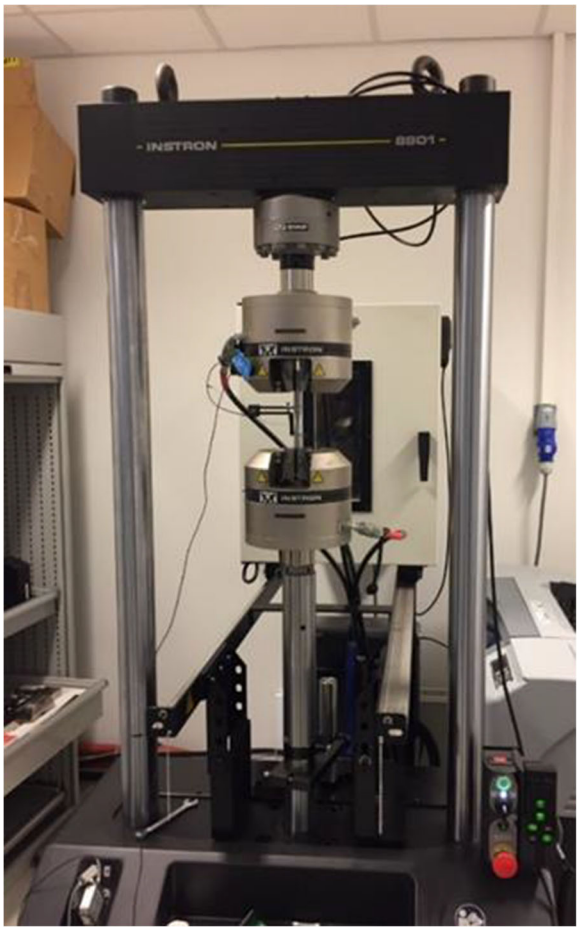

Fig. 4 Servo-hydraulic testing machine with elongated frame for climate chamber

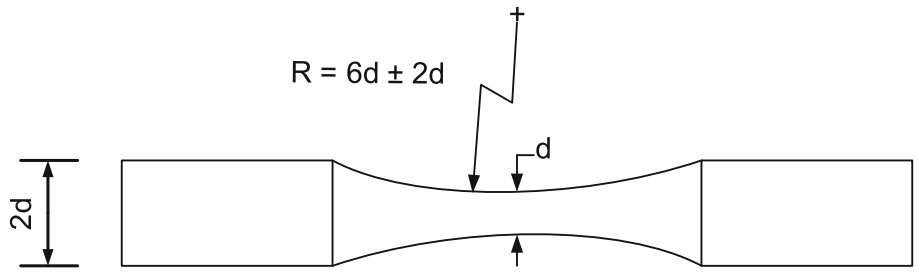

Fig. 5 Design of specimen for low-cycle fatigue based on Fig. 1 in ASTM E606/606M (2012). The geometry with hourglass shape was used in the experiments

integration, hourglass control). Example of the geometry and mesh are shown in Fig. 7a and b, respectively. The number of elements were ranging from 646 to 850 elements depending on the geometry of the specimens. The mesh quality was checked with the mesh control in FEM software (Abaqus) using the default settings with respect to corner angles and aspect ratio.

The deformation was applied in the longitudinal direction to the upper part of the model, representing the upper grip. All the other degrees of freedom were fixed for this part. The displacement was given as a linear function up to a chosen maximum limit of deformation. The part within the bottom grip was modeled to be free to move in the plane normal to the longitudinal axis. All the other degrees of freedom were fixed for this part.

The boundary conditions of the presented model over-constrain the rotation of the grips and under-constrain the sideways movement of the bottom grip. Geometrical imperfections and misalignment were not included in the model.

The essential output of this model is the critical buckling force, i.e., this is the force for the onset of sideways movement. The result of the sideways movement (buckling) is shown in Fig. 7c. The simulations of the model were run on a computer equipped with a processor of type Intel® Xeon® W-2123 CPU @ 3.60 GHz and 16-GB RAM. The CPU time for the simulations was ranging from about 1400 to 2300 s. Until the point of sideways movement, the mesh quality remained good.

The finite element model (Abaqus) calculated the sideways movement of the point RP-2 (see Fig. 7a) at the bottom plane of the specimen. The onset of sideways movement was determined by taking the time-derivative of the movement in the X- and Y-direction (U1 and U3 respectively) of the point RP-2 (see Fig. 7a). A typical example is shown in Fig. 8 for R5d8. The derivative of the movements in X-Z plane is stable prior to buckling. They fluctuate around zero, but when the derivative of the movement is drifting away from zero, the sideways movement had started. This represents the onset of buckling. For example, in Fig. 8, the onset of sideways movement determined by graphical analysis at time 0.24 s. The value is somewhat approximate, but the corresponding values in the force change little around this time in the data set. The compression force calculated from the finite element model (Abaqus) showed no significant change in value at the onset of sideways movement as can be seen in Fig. 9 for the exact same model as shown in Fig. 8. The strain energy from the finite element model was also analyzed and did not reveal a sign of sudden change at the onset of sideways movement of RP-2. Thus, there is no observed significant change in strain energy that indicates the onset of the buckling phenomenon observed.

Compression tests

Compression tests were done with a longitudinal extensometer and no transversal extensometer. The exact

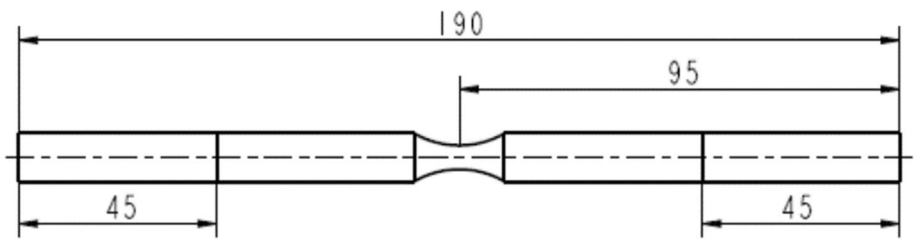

Fig. 6 Length of grip zone and compression zone in specimens tested. The 45 mm on the sides are confined within the grips of the machine. The end connections are straight sided collet-grip according to Fig. 5

Table 2 Geometries of tested specimens

Diameter d [mm]	Radius R [mm]	R/d
5	20	4
5	30	6
5	40	8
7	28	4
7	42	6
7	56	8

position of the thinnest section is difficult to locate in an hourglass-shaped specimen. Even a small misposition will influence the results as it is difficult to place a transversal mechanical extensometer on the exact place where the diameter is measured.

The experiments were designed to identify a critical force level on which the sideways movement of the specimens started. Therefore, the distance between the grips was set to 100 mm as can be seen from Fig. 6. This distance was marked with a marker on the specimens and introduced a small uncertainty for the experiment. A constant distance between the grips makes the experiments reproducible. Two specimens for each of the geometries described in Table 2 were tested.

The longitudinal extensometer was positioned in the parallel section outside the hourglass-shaped area. The measurement length of the extensometer was 50 mm. This makes the measurements from the tests reproducible as the diameter is constant at the two mounting points and the position of the mounting does not change as it is outside the area of plastic deformation. The extensometer measures both compression and elongation within the range of the instrument. The extensometer in use is documented with a linearity of 0.15% of full scale from the supplier Instron 2015 (reference manual). The setup is shown in Fig. 10.

The compression tests were force controlled. The tests had a power increase of 500 N/s up to the set maximum limit, which depended on the specimen geometry, and the critical buckling force calculated from the finite element model (Abaqus).

In order to identify the critical force for sideways movement, the experimental data need to be analyzed. The sideways movement is initiated by exceeding a critical force. In order to identify the onset of buckling, change in strain to force was analyzed by use of the following equation related to flexibility. Flexibility is derivative of displacement with respect to force, and this equation is correlated to flexibility

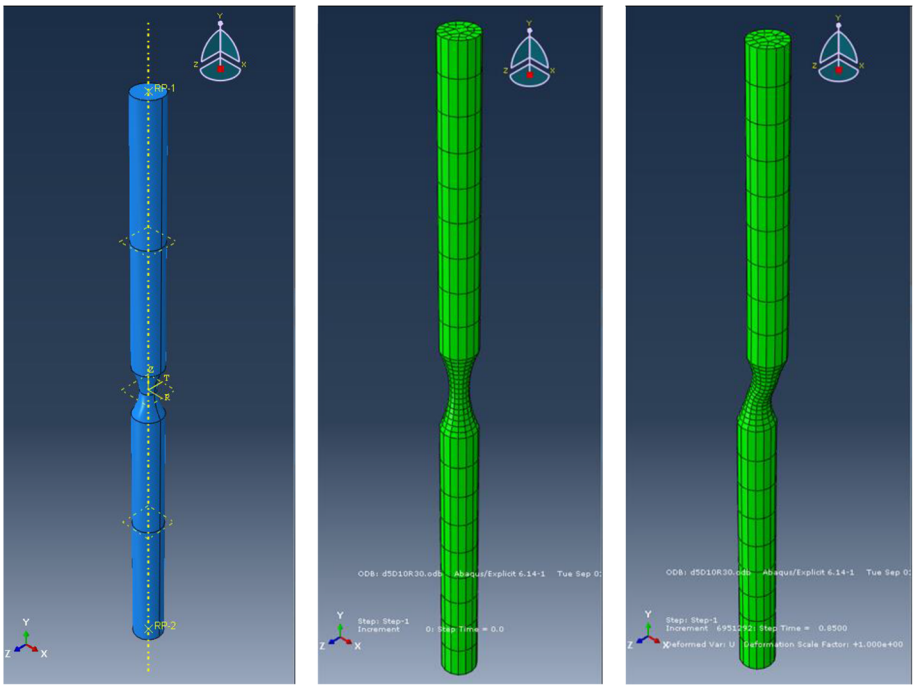

Fig. 7 **a** Modeled specimen geometry (the three yellow squares along the y-axis represent from the bottom upper part of lower grip, center plane of specimen and lower part of upper grip). **b** Finite element mesh of undeformed model. **c** Deformed model after onset of sideways movement (buckling)

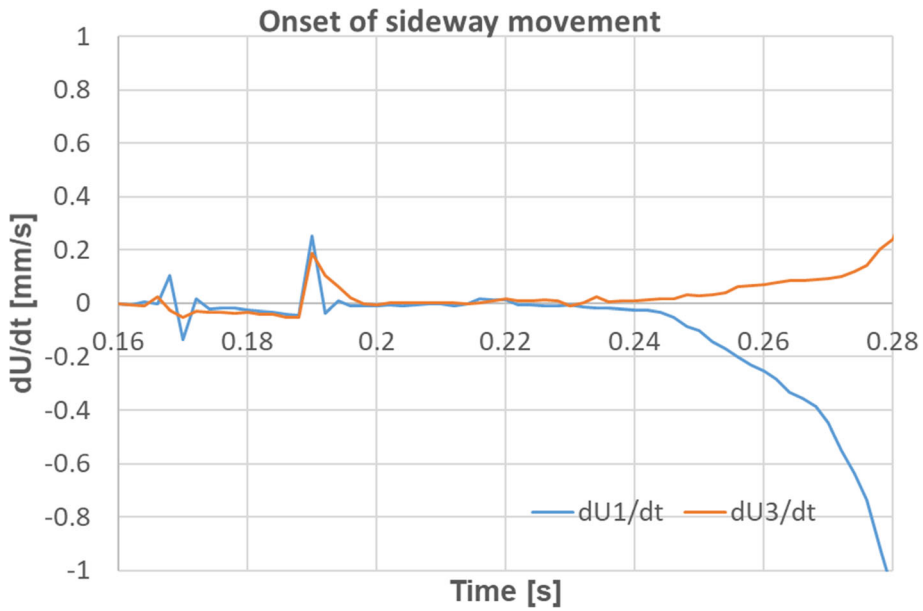

Fig. 8 Onset of sideways movement in specimen d5 with R/d = 6 according to Table 2. The onset of sideways movement is determined graphical at 0.24 s. U_1 and U_3 is the X- and Z-position of the point RP-2 in Fig. 7a

by a constant factor since displacement is replaced by strain.

$$\left|\frac{\Delta\varepsilon}{\Delta F}\right| = \left|\frac{\varepsilon_{i+1}-\varepsilon_i}{F_{i+1}-F_i}\right|$$

The number of datapoints for each specimen is typically above 4500, so the change from point to point is small. Therefore, the derivative gives a good indicator for changes both the force and the strain. The absolute value gives a more readable figure. A typical example of the critical force is given in Fig. 11. The geometry of this specimen can be seen in Table 2, with a smaller diameter of 7 mm and a radius of curvature of 56 mm.

The recorded data are somewhat noisy and no data filters are used. Here, the derivative shows the first clear peak which is interpreted as the critical force for onset of sideways movement. A closer look at the recorded

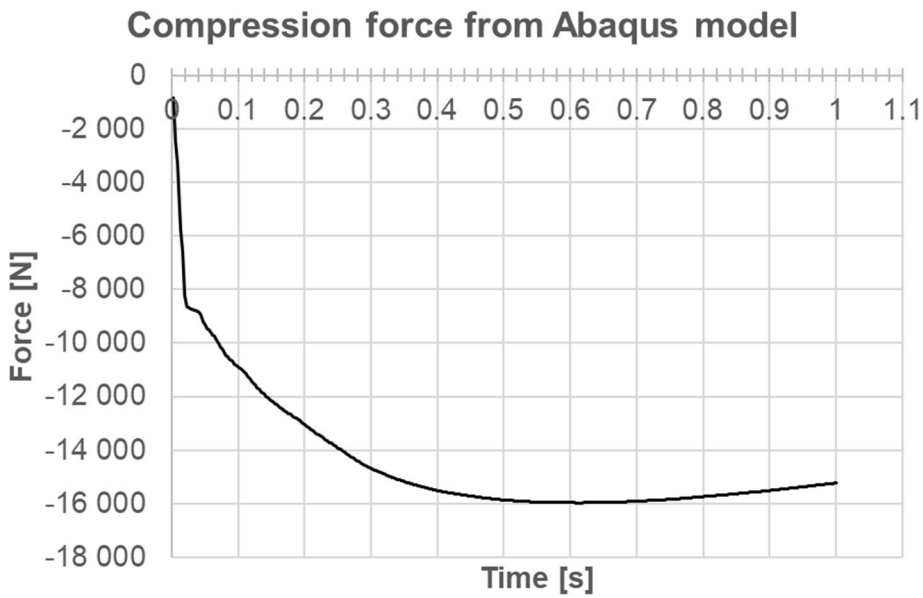

Fig. 9 Compression force versus time for specimen d5 with R/d = 6, calculated from the finite element model (Abaqus)

Fig. 10 Mounting of longitudinal extensometer

data shows that the maximum peak of the derivative is caused by a change in the measured longitudinal strain not followed by a corresponding change in force. This explains how the sideways movement appears. The derivative of the strain to force curve in Fig. 11 shows a clear peak at 22600 N. The corresponding force-displacement curve in Fig. 12 does not show any clear sign of onset of buckling.

Results and discussion

The model showed a reasonable correlation with the experimental results, as shown in Table 3. The deviation between the model and the experiments is maximum 11% between average of experiments and model. The model shows a significant better correlation for the larger diameter specimen. One can see from Table 3 that a larger diameter (d) gives a higher measured buckling force as expected. It is also clear that the smaller ratio R/d between the specimen diameter (d) and the radius of curvature (R) gives a higher buckling force.

A large diameter gives a smaller deviation between the experiment and the model. The model allows the whole bottom grip of the specimen to move freely in the X-Z plane. This is a simplification that does not include the stiffness with respect to sideways movement of the lower elongation rod of the test machine as can be seen from the photo in Fig. 4. This simplification is expected to give lower buckling force values in the model than in the experiments. In general, it is observed that the calculated values from the model are smaller than the measured values from the experiments.

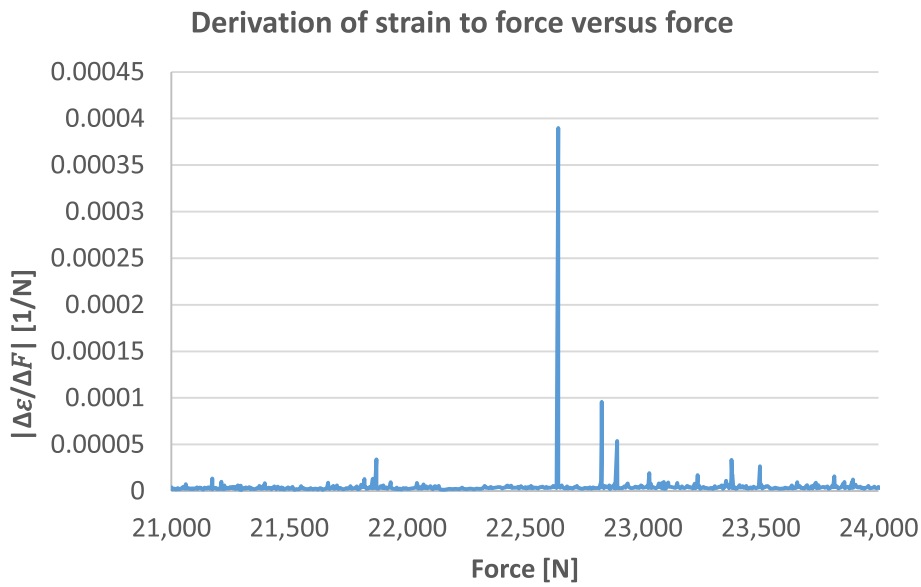

Fig. 11 Derivation of strain to compression force (flexibility) versus force in order to find critical force for sideways movement. The specimen had a diameter of 7 mm and R/d = 8

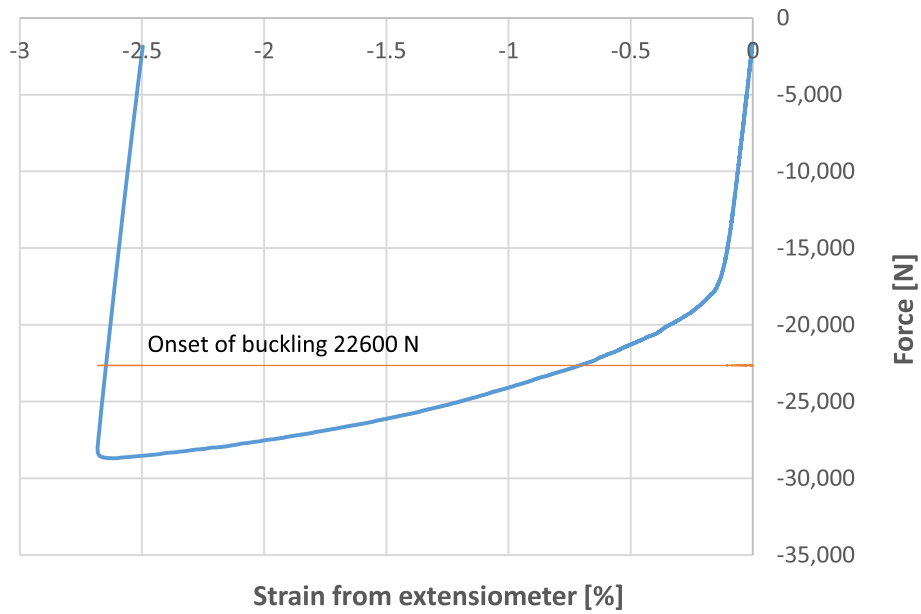

Fig. 12 Force-displacement curve for d = 7 mm and R/d = 8. Strain values are from extensometer. The critical buckling force is marked with the red line. Force and strain values are negative due to compression

This investigation was adopting a 3D model perfectly straight with the resultant of the force applied coinciding with the model's axis. The onset of buckling is normally caused by a perturbation for a perfectly straight model. In the current investigation, the perturbation is expected to be caused by a numerical effect in the calculations. Other factors influencing the onset of buckling could be tilting of the specimen or geometric imperfections in the shape of the specimen. By adapting a 0.1 and a 1° tilting of the specimen to the compression axis, the used model gave a lower buckling force than was found in the experiments. The determination of the degree of tilting will therefore cause a substantial uncertainty in the model. The same goes for the determination of the value of machine stiffness for predicting the onset of sideways movement of the specimen. Both these factors will influence the predicted buckling force.

The observed phenomenon named buckling in this work is principally different from a classic buckling. In those cases, the onset of sideways movement will lead to a reduction in measured force which will be at peak at the onset of buckling. In this case, the force is temporarily halting and continues to increase afterwards. The plateau in the force is less than a 1/10 of a second.

Table 3 Comparison of model with experiments

Smaller diameter, d [mm]	Radius of curvature R [mm]	Ratio R/d	Critical force, Pcr [kN]			Deviation between experiments and Finite element model (Abaqus) model
			Test 1	Test 2	Finite element model (Abaqus)	
5	20	4	18.42	17.09	15.81	− 11.0%
5	30	6	14.41	14.03	13.74	− 3.4%
5	40	8	12.61	12.94	11.83	− 7.4%
7	28	4	31.97	31.30	30.60	− 3.3%
7	42	6	26.46	26.70	26.52	− 0.2%
7	56	8	21.70	22.64	22.31	0.6%

Classic buckling is based on uniform diameter specimens and is thus not directly valid for hourglass-shaped specimens.

The method to determine the critical buckling force from the experiments used in this work is relatively simple compared to more expensive instrumentation like optical measurement methods with laser Hirose et al. (2000). The accuracy of the presented method is assumed to be high although it requires analysis of the data after the experiment is done.

The ability to predict the critical buckling load is essential for low-cycle fatigue testing in uniaxial mode. This requires availability of a model to predict the onset of buckling as this must be avoided during low-cycle fatigue testing in uniaxial mode.

During low-cycle fatigue testing, the material behavior will change. Before testing of an unknown material, it is uncertain to predict if the critical buckling load will increase or decrease compared to the first compression cycle as the model in this paper presents. In this case, an optical instrument might enable an in situ detection of a possible sideways movement. Independent of the material behavior, a low-cycle uniaxial fatigue test must start with a compression force below the buckling force.

Conclusion

A model for predicting buckling of hourglass-shaped specimen is presented. The model is calibrated based on tensile tests. A finite element software (Abaqus) is used to build the model. Compression tests of hourglassed specimen with diameters of 5 and 7 mm is done. The geometry of the specimens is based on the ASTM 606M standard. The ratio of the radius of curvature (R) in the hourglass section to the diameter (d) in the thinnest section (R/d) was tested at values 4, 6, and 8. A commercial cold-drawn low-carbon steel was used for the tests.

The model showed smaller deviation for the larger diameter (d) specimen. The smallest R/d-ratio gave the largest deviations between the model and the experiments. Specific knowledge about specimen geometry and the maximum planned compression force is necessary to avoid buckling during compression in axial low-cycle fatigue tests. The presented work is limited to the first compression cycle, but is crucial for a successful low-cycle fatigue test.

Acknowledgements

The authors are thankful for assistance in the laboratory at Department of Mechanical Engineering at Western Norway University of Applied Sciences. Mr. Harald Moen operated the tensile machine, and the specimens are machined by Mr. Kjetil Gravelseter. A special thanks to the faculty of Engineering and Science that has financed IAESTE-practitioners who have helped us in this work.

Authors' contributions

VH did the modeling work in the finite element software and analyzed the experiments in a spreadsheet. During this work, he was supervised by ØF and RG. The manuscript is prepared and written by RG and ØF in partnership. The authors read and approved the final manuscript.

Funding

This investigation is funded by internal resources at the faculty if engineering and science at Western Norway University of Applied Sciences.

Availability of data and materials

All the data used in this investigation are available on request from the corresponding author.

Declarations

Competing interests

The authors declare that they have no competing interests.

Author details

[1]Mechanical Engineering, Western Norway University of Applied Sciences, 5063 Bergen, Norway. [2]Civil Engineering, Western Norway University of Applied Sciences, 5063 Bergen, Norway. [3]Department of Machine Parts and Mechanisms, Technical University of Ostrava VSB, 70800 Ostrava, Czech Republic.

Received: 27 October 2020 Accepted: 3 June 2021
Published online: 29 June 2021

References

ASTM E606/606M (2012) Standard test method for strain-controlled fatigue testing, (West Conshohocken, PA: ASTM International, approved 2012). https://doi.org/10.1520/E0606_E0606M-12

EN 10025-1 (2004), Hot rolled products of structural steels. Part 1: general technical delivery conditions.

Hales R, Holdsworth S. R, O'Donnell M. P., Perrin I. J & Skelton R. P, (2014) "A code of practice for the determination of cyclic stress-strain data," Materials at high temperatures, 19, no 4, 165-185, https://doi.org/10.1179/mht.2002.022

Hirose T., Sakasegawa H., Kohyama A., Katoh Y., Tanigawa H, (2000) "Effect of specimen size on fatigue properties of reduced activation ferritic/martensitic steels", Journal of Nuclear Materials, 283-287, 1018-1022, https://doi.org/10.1016/S0022-3115(00)00141-0

Hu Xiaoyu, Wagoner Robert H., Daehn Glenn S. and Ghosh Somnath, (1994) Comparison of explicit and implicit finite element methods in the quasistatic simulation of uniaxial tension, *Communications in Numerical Methods in Engineering, vol. 10*, 993- 1003, https://doi.org/10.1002/cnm.1640101205, 12

Instron, Reference manual equipment M25-16655-EN revision A, 2620-600 series dynamic strain gauge extensiometer, Appendix A-1 (2015)

Narendra PV, Prasad K, Krishna EH, Kumar V, Singh KD, (2019) "Low-cycle-fatigue (LCF) behavior and cyclic plasticity modeling of E250A mild steel," *Structures 20*: 594-606, https://doi.org/10.1016/j.istruc.2019.06.014

Nogami, S., Sato, Y., Tanaka, A., Hasegawa, A., Nishimura, A., & Tanigawa, H. (2010). Effect of specimen shape on the low-cycle fatigue life of reduced activation ferritic/martensitic steel. *Journal of Nuclear Science and Technology*, *47*(1), 47–52. https://doi.org/10.1080/18811248.2010.9711926.

Sandhya R, Veeramani A, Bhanu Sankara Rao K. and Mannan S. L (1994), "On specimen geometry effects in strain controlled low-cycle fatigue," *Fatigue 16*, no 3: 202-208, https://doi.org/10.1016/0142-1123(94)90004-3

Skelton, R. P. (2013). Low-cycle fatigue specimen design, hardening, softening and strain concentration effects at elevated temperatures. *Materials at High Temperatures*, *30*(2), 99–116 https://doi.org/10.3184/096034013X13721793212862.

Romanova V, Balokhonov R, Emelianova E, Zinovieva O, Zinoviev A, (2019) Microstructure-based simulations of quasistatic deformation using an explicit dynamic approach, Facta universitatis Series: Mechanical Engineering Vol. 17, No 2, pp. 243 - 254 https://doi.org/10.22190/FUME190403028R

Publisher's Note